Journal of Hydrology 512 (2014) 442–446

Contents lists available at ScienceDirect

Journal of Hydrology

journal homepage: www.elsevier.com/locate/jhydrol

Technical Note

Moisture-pressure dynamics above an oscillating water table

Nick Cartwright *

Griffith School of Engineering, Gold Coast Campus, Griffith University, Queensland 4222, Australia

ARTICLE INFO

Article history:
Received 11 November 2013
Received in revised form 6 March 2014
Accepted 7 March 2014
Available online 19 March 2014
This manuscript was handled by Corrado Corradini, Editor-in-Chief, with the assistance of Fritz Stauffer, Associate Editor

Keywords:
Oscillating water table
Unsaturated flow
Hysteresis

SUMMARY

This paper presents a sand column dataset on the soil moisture-pressure dynamics above a simple harmonic oscillating water table. A total of 19 experiments were conducted in which all experimental parameters were held constant except for the oscillation period which ranged between 12.25 h down to 10 s. The data show clear evidence of hysteresis at longer oscillation periods where the unsaturated zone has sufficient time to adjust to the water table motion. At shorter periods the contrary exists with the extent of moisture-pressure variations greatly reduced and, for periods less than 15 min, the dynamics become non-hysteretic. The high frequency moisture-pressure loops, although non-hysteretic, do not follow the (non-hysteretic) static equilibrium wetting or drying curves but are consistent with the scanning loops generated by a commonly adopted hysteresis algorithm for numerical solution of the Richards (1931) equation. Thus, the data provides new physical insights behind the need to include hysteresis effects when simulating high frequency water table motions as found by previous researchers.

1. Introduction

The influence of the unsaturated zone on periodic water table dynamics is widely recognised in the literature (e.g. Barry et al., 1996; Cartwright et al., 2005, 2009; Lehman et al., 1998; Li et al., 1997; Nielsen and Perrochet, 2000a,b; Stauffer and Kinzelbach, 2001; Werner and Lockington, 2003). This is particularly the case with high frequency water table fluctuations which in turn have been linked to the mobility of sediments on beaches (e.g. Elfrink and Baldock, 2002) and also play a role in modifying the patterns of salt-water intrusion into coastal aquifers (Xin et al., 2010). This paper presents new sand column experiments on the moisture-pressure dynamics above a simple harmonic oscillating water table which reveal new insights into the influence of hysteresis on the response of the unsaturated zone.

Lehman et al. (1998) conducted sand column experiments in which periodic sawtooth shaped forcing was applied to the base of the sand where the pressure head oscillated between +1 cm and −24 cm relative to the base of the column. The moisture-pressure response was then observed in the sand for two test cases with varying oscillation periods: 180 min and 33 min. Their data illustrated a strong asymmetry in the moisture content response to the symmetric forcing condition due to hysteresis effects which was confirmed by the need to include the hysteresis theory of Mualem (1984) in their numerical solution of the Richards (1931) equation in order to reproduce the data.

Stauffer and Kinzelbach (2001) also conducted sand column experiments using periodic forcing conditions at the base. However, due to slow response times of the tensiometers used, they were unable to closely examine the moisture pressure dynamics and instead focussed on the moisture dynamics alone which were measured using the gamma probe technique. They also confirmed the need to include hysteresis effects in the solution of the Richards (1931) equation in order to reproduce their moisture data.

The present paper extends this previous research by presenting data on the moisture-pressure dynamics above a periodically oscillating water table over a wide range of frequencies. The new data consist of co-located moisture and pressure measurements which facilitate the opportunity to examine the moisture-pressure scanning loops above the water table which provides important new physical insights into unsaturated groundwater dynamics with particular relevance to ocean-aquifer coupling.

2. Sand column experiments

The 1.6 m high sand column used in the present experiments is illustrated in Fig. 1 and is the same as described in detail by Nielsen and Perrochet (2000a,b) and Cartwright et al. (2005, 2009). At the base of the sand column was a porous plate separating the sand above from a clear water cell below which was connected to an external overflow reservoir which delivered a simple harmonic

* Tel.: +61 (0)7 5552 9214.
E-mail address: n.cartwright@griffith.edu.au

http://dx.doi.org/10.1016/j.jhydrol.2014.03.024
0022-1694/

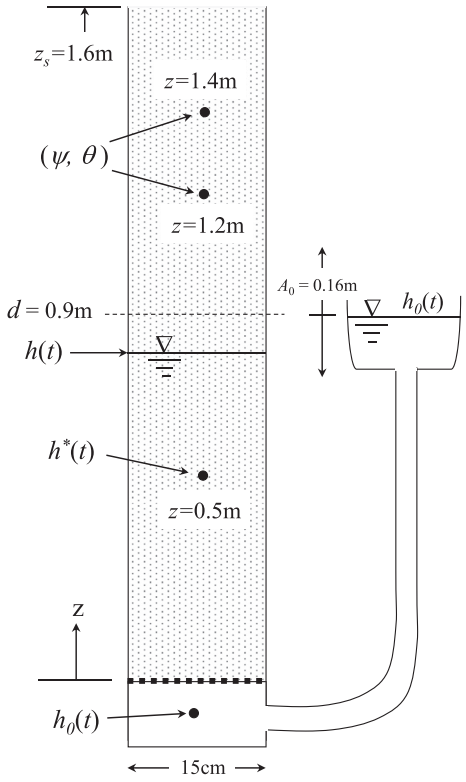

Fig. 1. Schematic illustration of the sand column and monitoring locations.

driving head ($h_0 = d + A\cos\omega t$) at the base of the sand. A total of 19 experiments were conducted in which the forcing parameters were fixed with a mean driving head level of $d = 0.9$ m, a driving head amplitude of $A = 0.16$ m. The only variable was the oscillation period (T) that varied between from 12.25 h to 10 s.

The clear water driving head pressure at the base of the sand and the pressure in the saturated zone ($h^*(z = 0.5\text{ m})$) were measured using transducers connected to stainless steel piezometers extending horizontally into the column. This saturated zone pressure measurements was used to compute the water table elevation following Nielsen and Perrochet (2000a,b),

$$h(t) = \frac{z h_0(t)}{z + h_0(t) - h^*(z,t)} \quad (1)$$

At two locations in the unsaturated zone ($z = 1.2$ m and 1.4 m), the instantaneous moisture-pressure dynamics were measured by co-locating a UMS-T5 tensiometer and an MP406 standing wave type moisture content probe. The sediment was fine grained quartz sand whose hydraulic properties are provided in Table 1.

It is noted that the experimental setup was such that any influence of truncation of the capillary fringe due to the presence of the sand surface on the water table dynamics was negligible. Cartwright et al. (2004) demonstrated using a similar sand column setup that truncation effects became significant for $z_s \leq h_{max} + 0.5H_\psi$ Adopting the worst case scenario for the present experiments by assuming $h_{max} + 0.5H_\psi = d + A + 0.5H_\psi = 1.26$ m then, with $z_s = 1.6$ m, any truncation effects did not influence the data.

For each oscillation period the system was allowed to run until a steady oscillatory state was reached as determined by the stabilisation of harmonic parameters (amplitudes and phases) in consecutive oscillation periods. The ensuing analysis and discussions in this paper are based on the final steady oscillatory state.

Table 1
Summary of experimental parameters.[a]

d, m	A, m	K, m/s	θ_s	θ_r	α^d, m^{-1}	β	ζ
0.9	0.16	2.00×10^{-4}	0.355	0.03	2.3	10	1.7

[a] d and A are the mean and amplitude of the driving head. K is the saturated hydraulic conductivity (after Cartwright et al., 2009). θ_s and θ_r are the saturated and residual moisture contents where θ_s was taken to be the maximum reproducible value of θ for the $T = 12.25$ h test data. α^d and β are the best fit *van Genuchten* parameters for the first drying curve (after Nielsen and Perrochet, 2000a,b). $\zeta = \alpha^w/\alpha^d$ is the adopted hysteresis ratio after Kool and Parker (1987).

3. Results and discussion

Fig. 2 presents the observed moisture-pressure dynamics for 12 experiments with oscillation periods ranging from $T = 12.52$ h to $T = 75$ s. For comparison the static wetting and drying curves based on the best-fit van Genuchten (1980) parameters provided in Table 1 are also shown. For shorter oscillation periods, there was no dynamic response of the moisture and pressure and thus data are not presented.

3.1. Experimental data

The data shown in Fig. 2 indicate a strong dependence of the moisture-pressure dynamics on the oscillation frequency. At the longest period of 12.25 h the dynamic loop at $z = 1.2$ m is seen to closely follow the static drying curve before disengaging for the wetting phase and ultimately joining the wetting curve prior to recommencing the drying phase. This is because, at low frequencies, there is sufficient time for the partially saturated zone to adjust to the slowly varying water table and an equilibrium balance between the moisture distribution and the water table is approached, especially at locations closer to the water table. At $z = 1.4$ m the nature of the loop is somewhat compressed with only a small difference in the wetting and drying paths.

As the oscillation period decreases distinct changes to the moisture-pressure loops are apparent. Firstly, the extent of moisture-pressure loops decreases as the period decreases because the damping of the water table increases with oscillation frequency ($A_{wt}/A_0 = 0.98$ for $T = 12.25$ h and $A_{wt}/A_0 = 0.44$ for $T = 75$ s, see also Cartwright et al. (2005)) in addition to the fact that there is relatively less time for the unsaturated zone to respond to the water table oscillations. Second, the hysteresis that is evident at longer periods gradually diminishes until, for $T \leq 15$ min, hysteresis is no longer apparent.

It is noted that the observed non-hysteretic scanning loops are distinctly different to the static equilibrium curves. This observation is consistent with previous modelling work which demonstrated the need to include hysteresis effects in numerical solutions of the Richards (1931) equation to match experimental data on high frequency water table motions (e.g. Lehman et al., 1998; Stauffer and Kinzelbach, 2001; Werner and Lockington, 2003). That is, even though the scanning loops themselves are observed to be non-hysteretic for high frequency oscillations, the deviation of the scanning loops from the static wetting and drying curves can only be captured in the model using a hysteresis scanning loop algorithm (e.g. Scott et al., 1983). This will be confirmed further in Section 3.2.

Also shown in Fig. 2, is a "best-fit" non-hysteretic van Genuchten (1980) curve using $\beta = 3$ which follows on from the modelling results of Cartwright et al. (2005) who demonstrated that, whilst using the first drying curve value of $\beta = 10$ in a non-hysteretic Richards (1931) equation model was unable to predict their sand column data, curiously a non-hysteretic $\beta = 3$ curve could. The data

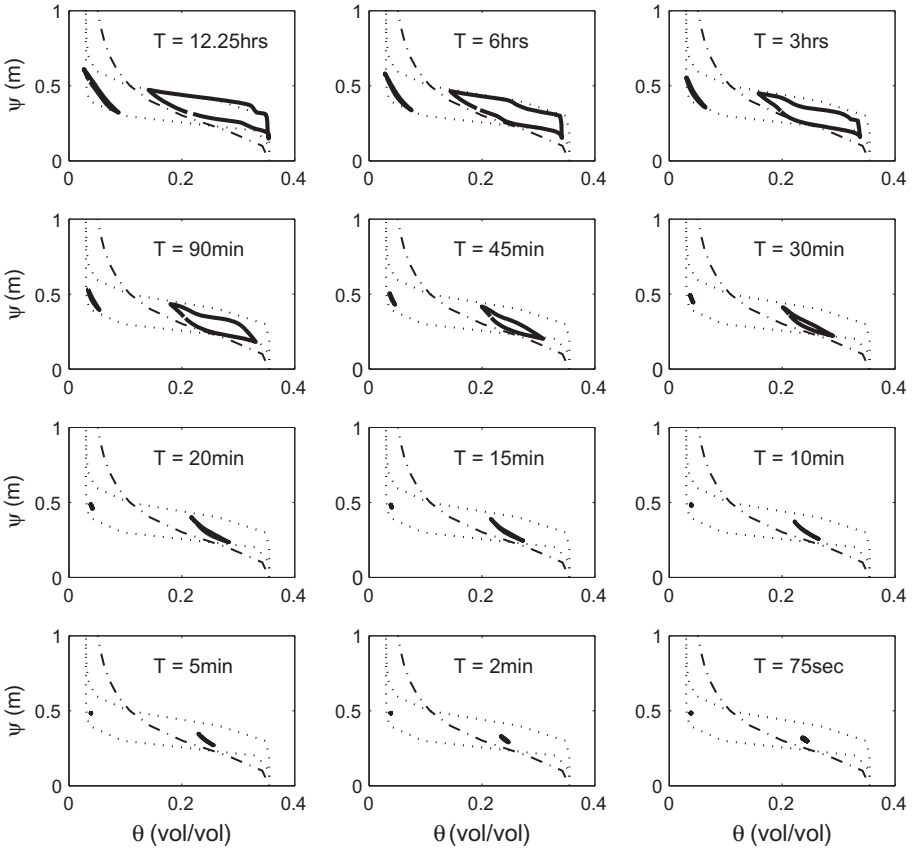

Fig. 2. Observed moisture-pressure relationships (bold solid lines) for a full oscillation period at $z = 1.2$ m and 1.4 m. Each panel corresponds to a different oscillation period as indicated. The dashed lines denote the equilibrium van Genuchten (1980) curves (drying and wetting) based on parameters given in Table 1. The dash–dot curve is an indicative van Genuchten (1980) curve with $\beta = 3$.

in Fig. 2 indicates that, when the period decreases, the slope of the (non-hysteretic) moisture-pressure scanning loops is closely matched by the slope of the $\beta = 3$ curve. In other words, for high frequency motion, the capillary capacity ($c(\psi) = \mathrm{d}\theta/\mathrm{d}\psi$) of a non-hysteretic $\beta = 3$ curve is more representative of the observed moisture-pressure relationship than a non-hysteretic curve based on static equilibrium measurements (corresponding to $\beta = 10$). For longer period motion, the observed capillary capacity is reasonably well captured by the static equilibrium curves hence the reason why long period water table motions are adequately described without consideration of hysteresis (e.g. Werner and Lockington, 2003).

3.2. Numerical modelling

The Hydrus 1D model was used to solve the Richards (1931) equation for flow through unsaturated porous media,

$$\frac{\partial\theta}{\partial t} = \frac{\partial}{\partial z}\left(K(\psi)\frac{\partial\psi}{\partial z}\right) \tag{2}$$

where θ is the volumetric soil moisture content, z is the elevation head, ψ is the water pressure head and $K(\psi)$ is the unsaturated hydraulic conductivity.

Introduction of the capillary capacity term,

$$c(\psi) = \frac{d\theta}{d\psi} \tag{3}$$

into Eq. (2) yields,

$$c(\psi)\frac{\partial\psi}{\partial t} = \frac{\partial}{\partial z}\left(K(\psi)\frac{\partial\psi}{\partial z}\right) \tag{4}$$

Solution of Eq. (2) requires knowledge of both the moisture-pressure function $\theta(\psi)$ and the unsaturated hydraulic conductivity function $K(\theta)$. The moisture-pressure model adopted in this study are the van Genuchten (1980) functions,

$$S_e = \frac{\theta - \theta_r}{\theta_s - \theta_r} = \left[\frac{1}{1 + (\alpha\psi)^{\beta}}\right]^m \tag{5}$$

where S_e is the effective saturation, θ_r and θ_s are respectively the residual and saturated moisture contents and α, β and m (=1–1/β) are curve fitting parameters. The corresponding hydraulic conductivity function is,

$$K_r = \frac{K(\theta)}{K_S} = \sqrt{S_e}\left\{1 - \left[1 - S_e^{1/m}\right]^m\right\}^2 \tag{6}$$

where K_r and K_s are respectively the relative and saturated hydraulic conductivities.

The hysteresis model employed by Hydrus 1D is based on the empirical model of Scott et al. (1983) which was modified to account for air entrapment by Kool and Parker (1987) and then further modified by Vogel et al. (1996) to consider hysteresis in the hydraulic conductivity function. For brevity here, the reader is referred to Vogel et al. (1996) or Šimůnek et al. (2009) for details.

Fig. 3 presents the simulated moisture-pressure dynamics for the same 12 experiments shown previously in Fig. 2 with

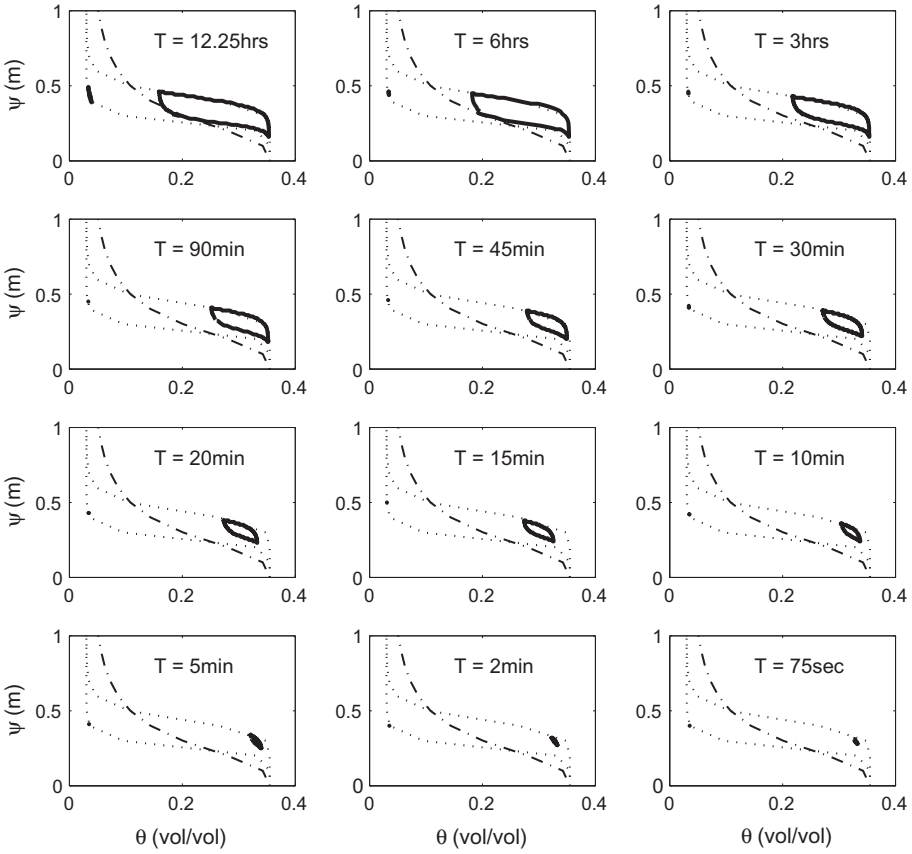

Fig. 3. Simulated moisture-pressure relationships (bold solid lines) at $z = 1.2$ m and 1.4 m. Each panel corresponds to a different oscillation period as indicated. The dashed lines denote the equilibrium van Genuchten (1980) curves (drying and wetting) based on parameters given in Table 1. The dash–dot curve is an indicative van Genuchten (1980) curve with $\beta = 3$. Simulations used the hydraulic parameters given in Table 1 and bottom forcing parameters of $A_0 = 0.15$ m and $d = 0.9$ m.

oscillation periods ranging from $T = 12.52$ h to $T = 75$ s. For comparison the static wetting and drying curves based on the best-fit van Genuchten (1980) parameters provided in Table 1 are also shown. For shorter oscillation periods, there was no dynamic response of the moisture and pressure and thus data are not presented.

The model is able to capture the same general features observed in the data (refer to Fig. 2 for corresponding experimental data). As the oscillation period decreases then (a) there is a reduction in the extent of the moisture-pressure loops and (b) the loops become non-hysteretic albeit deviating from the non-hysteretic static equilibrium curves. A summary of RMS errors for each simulation is provided in Table 2 where small quantitative differences with the data are apparent but these are likely due to the uncertainty in parameter estimation.

Table 2
Summary of RMS Errors for model predictions.[a]

T	$z = 1.2$ m		$z = 1.4$ m	
	ψ (m)	θ (vol/vol)	ψ (m)	θ (vol/vol)
12.25 h	0.011	0.015	0.096	0.026
6 h	0.015	0.026	0.092	0.020
3 h	0.015	0.050	0.071	0.016
90 min	0.011	0.041	0.035	0.008
45 min	0.016	0.069	0.027	0.008
30 min	0.012	0.064	0.060	0.006
20 min	0.016	0.056	0.045	0.006
15 min	0.015	0.057	0.025	0.009
10 min	0.017	0.079	0.062	0.004
5 min	0.017	0.088	0.074	0.004
2 min	0.016	0.087	0.084	0.003
75 s	0.015	0.089	0.085	0.003

[a] T is the oscillation period, z is the measurement elevation, ψ is the pressure head and θ is the volumetric moisture content.

4. Conclusions

New sand column experiments have been conducted to examine the moisture-pressure dynamics above a periodically oscillating water table. For long oscillation periods, the moisture profile in the unsaturated zone has more time to respond to the water table motion and exhibits behaviour similar to that described by the static, equilibrium moisture-pressure relationships.

For shorter oscillation periods, the water table oscillations become more damped and there is relatively less time for the unsaturated zone to adjust to the fast moving water table and so the moisture-pressure loops show a greatly reduced extent and become non-hysteretic for $T \leq 15$ min. The high frequency loops show significant departure from the static equilibrium curves and provide new physical insights behind the need to include hysteresis effects in numerical models to accurately predict high frequency water table motions.

The data also indicates that the capillary capacity for the high frequency loops is more closely represented by the capillary capacity found using a van Genuchten (1980) curve with $\beta = 3$ as opposed to the static equilibrium value of $\beta = 10$. This provides some physical basis to explain how previous sand column experiments on high frequency water table motion can be predicted using a non-hysteretic Richards (1931) model with a "magical" $\beta = 3$ curve (Cartwright et al., 2005).

References

Barry, D.A., Barry, S.J., Parlange, J.-Y., 1996. Capillarity correction to Periodic solutions of the shallow flow approximation. In: Pattiaratchi, C.B. (Ed.), Mixing in Estuaries and Coastal Seas. Coastal and Estuarine Studies, AGU, Washington DC, pp. 496–510.

Cartwright, N., Nielsen, P., Li, L., 2004. Experimental observations of watertable waves in an unconfined aquifer with a sloping boundary. Adv. Water Resour. 27, 991–1004.

Cartwright, N., Nielsen, P., Perrochet, P., 2005. The influence of capillarity on a simple harmonic oscillating water table: sand column experiments and modelling. Water Resour. Res. 41 (8), W08416.

Cartwright, N., Nielsen, P., Perrochet, P., 2009. Behaviour of a shallow watertable under periodic flow conditions. Water Resour. Res. 45 (W03416).

Elfrink, B., Baldock, T.E., 2002. Hydrodynamics and sediment transport in the swash zone: a review and perspectives. Coast. Eng. 45 (3), 149–167.

Kool, J.B., Parker, J.C., 1987. Development and evaluation of closed-form expressionbs for hysteretic soil hydraulic properties. Water Resour. Res. 23 (1), 105–114.

Lehman, P., Stauffer, F., Hinz, C., Dury, O., Flühler, H., 1998. Effect of hysteresis on water flow in a sand column with a fluctuating capillary fringe. J. Contam. Hydrol. 33 (1–2), 81–100.

Li, L., Barry, D.A., Parlange, J.-Y., Pattiaratchi, C.B., 1997. Beach water table fluctuations due to wave run-up: capillarity effects. Water Resour. Res. 33 (5), 935–945.

Mualem, Y., 1984. A modified dependent-domain theory of hysteresis. Soil Sci. 137 (5), 283–291.

Nielsen, P., Perrochet, P., 2000a. Watertable dynamics under capillary fringes: experiments and modelling. Adv. Water Resour. 23 (1), 503–515.

Nielsen, P., Perrochet, P., 2000b. ERRATA: Watertable dynamics under capillary fringes: experiments and modelling (Advances in Water Resources 23 (2000) 503–515). Adv. Water Resour. 23, 907–908.

Richards, L.A., 1931. Capillary conduction of liquids through porous medium. Physics 1, 318–333.

Scott, P.S., Farquhar, G.J., Kouwen, N., 1983. Hysteresis effects on net infiltration. Advances in Infiltration. Am. Soc. Agri. Eng. 11–83, 163–170.

Šimůnek, J., Šejna, M., Saito, H., Sakai, M., van Genuchten, M.T., 2009. The HYDRUS-1D Software Package for Simulating the One-Dimensional Movement of Water, Heat, and Multiple Solutes in Variably-Saturated Media, Version 4.08.

Stauffer, F., Kinzelbach, W., 2001. Cyclic hysteretic flow in porous medium column: model, experiment, and simulations. J. Hydrol. 240 (3–4), 264–275.

van Genuchten, M.T., 1980. A closed form equation for predicting the hydraulic conductivity of unsaturated soils. Soil Sci. Soc. Am. J. 44, 892–898.

Vogel, T., Huang, K., Zhang, R., van Genuchten, M.T., 1996. The HYDRUS code for simulating one-dimensional water flow, solute transport, and heat movement in variably-saturated media, Version 5.0 140, U.S. Salinity Laboratory, USDA, ARS, Riverside, CA.

Werner, A.D., Lockington, D.A., 2003. Influence of hysteresis on tidal capillary fringe dynamics in a well-sorted sand. Adv. Water Resour. 26 (11), 1199–1204.

Xin, P., Robinson, C., Li, L., Barry, D.A., Bakhtyar, R., 2010. Effects of wave forcing on a subterranean estuary. Water Resources Res. 46.